The Fourier-Slice Theorem

The relationship relating the 1-D Fourier transform of a projection and the 2-D Fourier transform of the region from which the projection was obtained is the basis for reconstruction methods capable of dealing with the blurring problem.

The 1-D Fourier transform of a projection with respect to ρ is

$$G(\omega,\theta) = \int_{-\infty}^{\infty} g(\rho,\theta)\, e^{-j2\pi\omega\rho} d\rho \qquad (5.11\text{-}8)$$

where ω is the frequency variable, and this expression is for a given value of θ.

Substituting

$$g(\rho,\theta) = \int_{-\infty}^{\infty}\int_{-\infty}^{\infty} f(x,y)\delta(x\cos\theta + y\sin\theta - \rho)dxdy \qquad (5.11\text{-}3)$$

for $g(\rho,\theta)$ results the expression

$$\begin{aligned} G(\omega,\theta) &= \int_{-\infty}^{\infty}\int_{-\infty}^{\infty}\int_{-\infty}^{\infty} f(x,y)\,\delta(x\cos\theta + y\sin\theta - \rho)\, e^{-j2\pi\omega\rho} dxdyd\rho \\ &= \int_{-\infty}^{\infty}\int_{-\infty}^{\infty} f(x,y)\Big[\int_{-\infty}^{\infty} \delta(x\cos\theta + y\sin\theta - \rho)\, e^{-j2\pi\omega\rho} d\rho\Big] dxdy \\ &= \int_{-\infty}^{\infty}\int_{-\infty}^{\infty} f(x,y)\, e^{-j2\pi\omega(x\cos\theta + y\sin\theta)} dxdy \qquad (5.11\text{-}9) \end{aligned}$$

By letting $u = \omega\cos\theta$ and $v = \omega\sin\theta$, (5.11-9) becomes

$$G(\omega,\theta) = \Big[\int_{-\infty}^{\infty}\int_{-\infty}^{\infty} f(x,y)\, e^{-j2\pi(ux+vy)} dxdy\Big]_{u=\omega\cos\theta;\, v=\omega\sin\theta} \qquad (5.11\text{-}10)$$

We recognize (5.11-10) as the 2-D Fourier transform of $f(x,y)$ evaluated at the values of u and v indicated.

Equation (5.11-10) leads to

$$G(\omega,\theta) = [F(u,v)]_{u=\omega\cos\theta;v=\omega\sin\theta} = F(\omega\cos\theta,\omega\sin\theta), \quad (5.11\text{-}11)$$

which is known as the Fourier-slice theorem (or the projection-slice theorem).

The Fourier-slice theorem states that the Fourier transform of a projection is a slice of the 2-D Fourier transform of the region from which the projection was obtained.

This terminology can be explained with Figure 5.41.

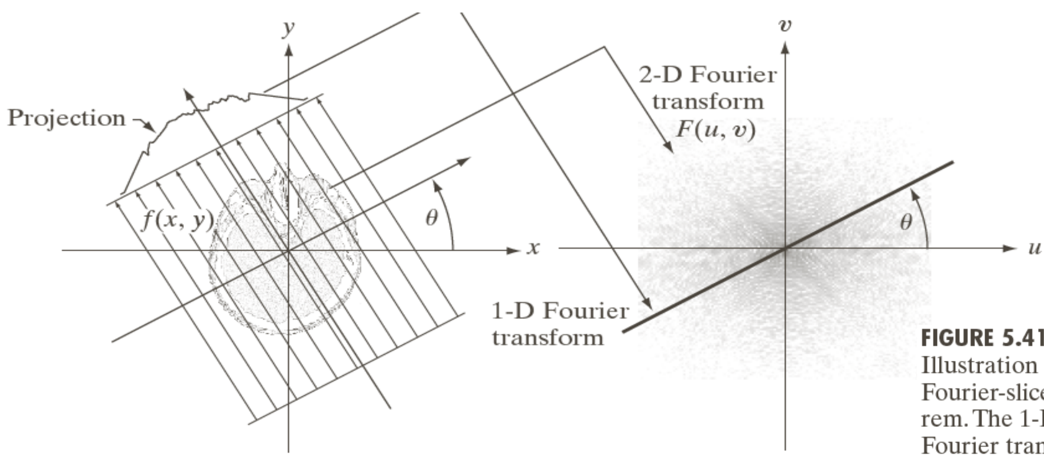

FIGURE 5.41 Illustration of the Fourier-slice theorem. The 1-D Fourier transform of a projection is a slice of the 2-D Fourier transform of the region from which the projection was obtained. Note the correspondence of the angle θ.

As Figure 5.41 shows, the 1-D Fourier transform of an arbitrary projection is obtained by extracting the values of $F(u,v)$ along a line oriented at the same angle as the angle used in generating the projection.

In principle, we could obtain $f(x,y)$ simply by obtaining the inverse Fourier transform $F(u,v)$, though it is expensive computationally with the involvement of inverting a 2-D transform.

Reconstruction Using Parallel-Beam Filtered Backprojections

Regarding to the blurred results, fortunately, there is a simple solution based on filtering the projections before computing the backprojections.

Recall

$$f(t,z) = \int_{-\infty}^{\infty}\int_{-\infty}^{\infty} F(\mu,\nu)e^{j2\pi(\mu t+\nu z)}d\mu d\nu\,, \qquad (4.5\text{-}8)$$

the 2-D inverse Fourier transform of $F(u,v)$ is

$$f(x,y) = \int_{-\infty}^{\infty}\int_{-\infty}^{\infty} F(u,v)e^{j2\pi(ux+vy)}du dv\,. \qquad (5.11\text{-}12)$$

As in (5.11-10) and (5.11-11), letting $u = \omega\cos\theta$ and $v = \omega\sin\theta$, we can express (5.11-12) in polar coordinates:

$$f(x,y) = \int_{0}^{2\pi}\int_{0}^{\infty} F(\omega\cos\theta,\omega\sin\theta)e^{j2\pi\omega(x\cos\theta+y\sin\theta)}\omega d\omega d\theta \qquad (5.11\text{-}13)$$

Then, using the Fourier-slice theorem, we have

$$f(x,y) = \int_{0}^{2\pi}\int_{0}^{\infty} G(\omega,\theta)e^{j2\pi\omega(x\cos\theta+y\sin\theta)}\omega d\omega d\theta\,. \qquad (5.11\text{-}14)$$

Using the fact that $G(\omega,\theta+\pi) = G(-\omega,\theta)$, we can express (5.11-14) as

$$f(x,y) = \int_{0}^{\pi}\int_{-\infty}^{\infty} |\omega| G(\omega,\theta)e^{j2\pi\omega(x\cos\theta+y\sin\theta)}d\omega d\theta\,. \qquad (5.11\text{-}15)$$

In terms of integration with respect to $|\omega|$, the term $x\cos\theta + y\sin\theta$ is a constant, which is recognized as ρ. Thus, (5.11-15) can be written as

$$f(x,y) = \int_{0}^{\pi}\left[\int_{-\infty}^{\infty} |\omega| G(\omega,\theta)e^{j2\pi\omega\rho}d\omega\right]_{\rho=x\cos\theta+y\sin\theta} d\theta\,. \qquad (5.11\text{-}16)$$

Recall

$$f(t) = \int_{-\infty}^{\infty} F(\mu) e^{j2\pi\mu t} d\mu \,, \qquad (4.2\text{-}17)$$

the inner expression in (5.11-16) is a 1-D inverse Fourier transform with the added term $|\omega|$.

Based on the discussion in Section 4.7, $|\omega|$ is a one-dimensional filter function.

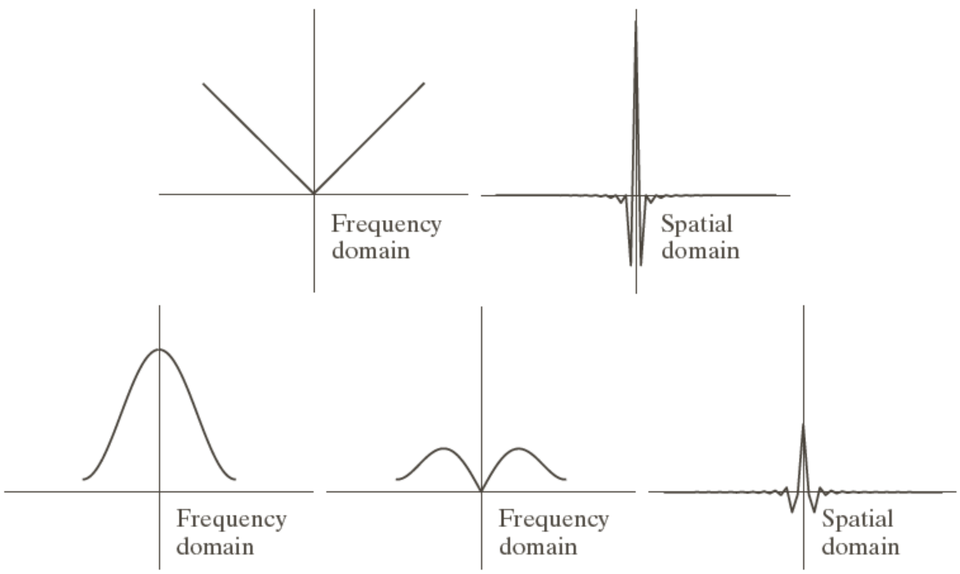

a b
c d e

FIGURE 5.42 (a) Frequency domain plot of the filter $|\omega|$ after band-limiting it with a box filter. (b) Spatial domain representation. (c) Hamming windowing function. (d) Windowed ramp filter, formed as the product of (a) and (c). (e) Spatial representation of the product (note the decrease in ringing).

$|\omega|$ is not integrable, because its amplitude extends to $+\infty$ in both directions, so the inverse Fourier transform is undefined.

In practice, the approach is to window the ramp so it becomes zero outside of defined frequency interval, as shown in Figure 5.42 (a).

Figure 5.42 (b) shows its spatial domain representation, obtained by computing its inverse Fourier transform. The resulting windowed filter exhibits noticeable ringing in the spatial domain. As discussed in Chapter 4, windowing with a smooth function will help in this situation.

An M-point discrete window function used frequently for implementation with the 1-D FFT is given by

$$h(\omega) = \begin{cases} c + (c-1)\cos\dfrac{2\pi\omega}{M-1} & 0 \le \omega \le (M-1) \\ 0 & \text{otherwise} \end{cases} \qquad (5.11\text{-}17)$$

When $c = 0.54$, this function is called the Hamming window.

Figure 5.42 (c) is a plot of the Hamming window, and Figure 5.42 (d) shows the product of this window and the band-limited ramp filter shown in Figure 5.42 (a).

Figure 5.42 (e) shows the representation of the product in the spatial domain, obtained by computing the inverse FFT.

Comparing Figure 5.42 (e) and Figure 5.42 (b), we can find that ringing was reduced in the window ramp.

On the other hand, because the width of the central lobe in Figure 5.42 (e) is slightly wider than that of Figure 5.42 (b), we would expect backprojections based on a Hamming window to have less ringing but be slightly more blurred.

Recalling

$$G(\omega,\theta) = \int_{-\infty}^{\infty} g(\rho,\theta)\, e^{-j2\pi\omega\rho}\, d\rho \qquad (5.11\text{-}8)$$

that $G(\omega,\theta)$ is the 1-D Fourier transform of $g(\rho,\theta)$, which is a single projection obtained at a fixed angle, θ.

Equation

$$f(x,y)=\int_0^{\pi}\left[\int_{-\infty}^{\infty}|\omega|\,G(\omega,\theta)\,e^{j2\pi\omega\rho}d\omega\right]_{\rho=x\cos\theta+y\sin\theta}d\theta \qquad (5.11\text{-}16)$$

states that the complete, back-projected image $f(x,y)$ is obtained as follows:

1. Compute the 1-D Fourier transform of each projection.
2. Multiply each Fourier transform by the filter function $|\omega|$, which has been multiplied by a suitable (e.g., Hamming) window.
3. Obtain the inverse 1-D Fourier transform of each resulting filtered transform.
4. Integrate (sum) all the 1-D inverse transform from Step 3.

This image reconstruction approach is called filtered backprojection.

In practice, because the data are discrete, all frequency domain computations are carried out using a 1-D FFT algorithm, and filtering is implemented using the same basic procedure explained in Chapter 4 for 2-D functions.

Example 5.19: Image reconstruction using filtered backprojections

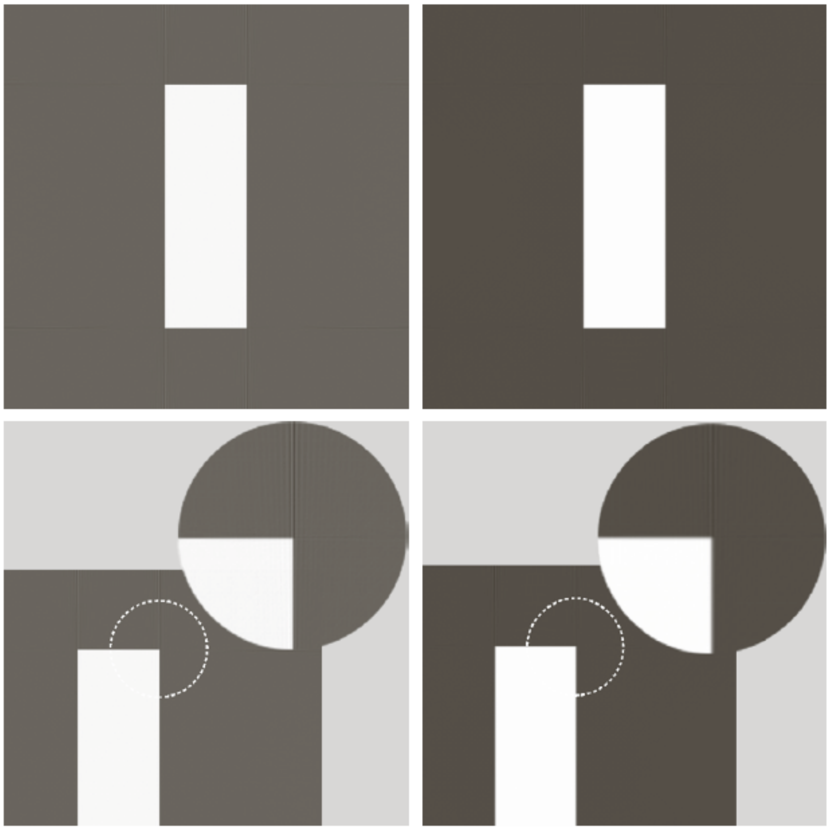

a b
c d

FIGURE 5.43 Filtered back-projections of the rectangle using (a) a ramp filter, and (b) a Hamming-windowed ramp filter. The second row shows zoomed details of the images in the first row. Compare with Fig. 5.40(a).

Figure 5.43 (a) shows the rectangle reconstructed using a ramp filter. The most vivid feature of this result is the absence of any visually detectable blurring. However, ringing is present, visible as faint lines, especially around the corners of the rectangle. Figure 5.43 (c) can show these lines in the zoomed section.

Using a Hamming window on the ramp filter helped considerably with the ringing problem, at the expense of slight blurring, as Figure 5.43 (b) and Figure 5.43 (d) show.

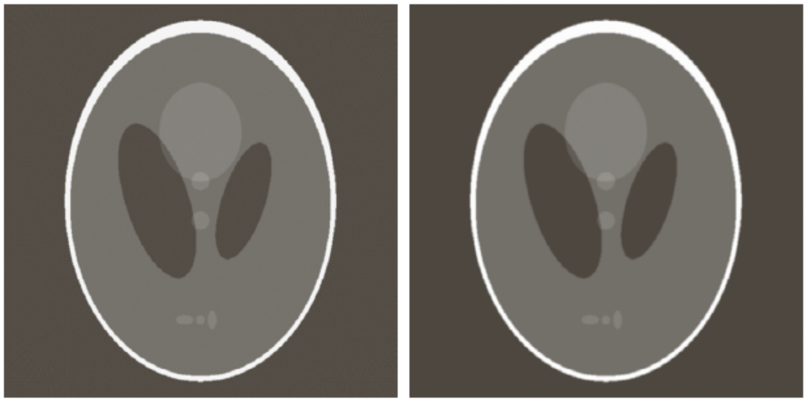

a b

FIGURE 5.44 Filtered backprojections of the head phantom using (a) a ramp filter, and (b) a Hamming-windowed ramp filter. Compare with Fig. 5.40(b).

The reconstructed phantom images shown in Figure 5.44 are from using the un-windowed ramp filter and a Hamming window on the ramp filter.

Since the phantom image does not have transitions that are sharp and prominent as the rectangle, so ringing is imperceptible in this case, though result shown in Figure 5.44 (b) is a slightly smooth than that of Figure 5.44 (a).

The discussion has been based on obtaining filtered backprojections via an FFT implementation. However, from the convolution theorem introduced in Chapter 4, we know that the equivalent results can be obtained using spatial convolution.

Note that the term inside the brackets in

$$f(x,y) = \int_0^{\pi}\left[\int_{-\infty}^{\infty} |\omega| G(\omega,\theta) e^{j2\pi\omega\rho} d\omega\right]_{\rho = x\cos\theta + y\sin\theta} d\theta \qquad (5.11\text{-}16)$$

is the inverse Fourier transform of the product of two frequency domain functions. According to the convolution theorem, they are equal to the convolution of the spatial representations (inverse Fourier transform) of these two functions.

Let $s(\rho)$ denote the inverse Fourier transform of $|\omega|$, we can write (5.11-16) as

$$\begin{aligned} f(x,y) &= \int_0^\pi \left[\int_{-\infty}^{\infty} |\omega| G(\omega,\theta) e^{j2\pi\omega\rho} d\omega\right]_{\rho=x\cos\theta+y\sin\theta} d\theta \\ &= \int_0^\pi [s(\rho)\star \ \mathrm{g}(\rho,\theta)]_{\rho=x\cos\theta+y\sin\theta}\, d\theta \\ &= \int_0^\pi \left[\int_{-\infty}^{\infty} \mathrm{g}(\rho,\theta)\, s(x\cos\theta + y\sin\theta - \rho) d\rho\right] d\theta \end{aligned} \tag{5.11-18}$$

The last two lines of (5.11-18) say the same thing: Individual backprojections at an angle θ can be obtained by convolving the corresponding projection, $\mathrm{g}(\rho,\theta)$, and the inverse Fourier transform of the ramp filter, $s(\rho)$.

With the exception of round off differences in computation, the results of using convolution will be identical to the results using FFT.

In general, convolution turns out to be more computationally efficient and is used in most of modern CT systems, while Fourier transform plays a central role in theoretical formulations and algorithm development.

5.11.6 Reconstruction Using Fan-beam Filtered Backprojections